Journal of the Korean Nuclear Society
Volume 32, Number 6, pp.566~594, December, 2000

Elevated Temperature Design of KALIMER Reactor Internals Accounting for Creep and Stress-Rupture Effects

Gyeong-Hoi Koo and Bong Yoo
Korea Atomic Energy Research Institute
150 Dukjin-dong, Yusong-gu, Taejon 305-353, Korea
ghkoo@kaeri.re.kr

(Received April 14, 2000)

Abstract

In most LMFBR(Liquid Metal Fast Breed Reactor) design, the operating temperature is very high and the time-dependent creep and stress-rupture effects become so important in reactor structural design. Therefore, unlike with conventional PWR, the normal operating conditions can be basically dominant design loading because the hold time at elevated temperature condition is so long and enough to result in severe total creep ratcheting strains during total service lifetime. In this paper, elevated temperature design of the conceptually designed baffle annulus regions of KALIMER(Korea Advanced Liquid MEtal Reactor) reactor internal structures is carried out for normal operating conditions which have the operating temperature 530℃ and the total service lifetime of 30 years. For the elevated temperature design of reactor internal structures, the ASME Code Case N-201-4 is used. Using this code, the time-dependent stress limits, the accumulated total inelastic strain during service lifetime, and the creep-fatigue damages are evaluated with the calculation results by the elastic analysis under conservative assumptions. The application procedures of elevated temperature design of the reactor internal structures using ASME Code Case N-201-4 with the elastic analysis method are described step by step in detail. This paper will be useful guide for actual application of elevated temperature design of various reactor types accounting for creep and stress-rupture effects.

Key Words : elevated temperature design, inelastic strain, creep-fatigue damage, elastic analysis method, stress relaxation strength

1. Introduction

In general, the operating temperature of conventional PWR(Pressurized Water Reactor) is under 350℃, therefore the creep or ratcheting behavior are not severe in the reactor internal structures and the stress and fatigue limits are mainly checked to assure the structural design integrity by the design rules such as ASME Boiler and Pressure Vessel Code Section III, Subsection NG[1]. When the metal temperature exceeds the upper limits of ASME Code Subsection NG, the modifications and additions to Subsection NG rules are necessary to account for the time

dependent creep and stress-rupture effects.

For most LMFBR(Liquid Metal Fast Breed Reactor) designs using sodium coolant, the operating temperature exceeds 500℃ and the design pressure is so low under 5bar. Even though the sodium-cooled reactor has a great advantage such that any structural deterioration is progressive, not sudden due to lower operating pressure, the time dependent creep and ratchet behavior can be severely occurred in reactor internal structures due to elevated temperature operation. In elevated temperature design, the parameters such as hold temperature, hold time duration, and number of stress cycles are very important to calculate the total accumulated inelastic strain and the creep-fatigue damages. Unlike with PWR design, these time dependent factors should be carefully considered in stage of the design by analysis. For elevated temperature design of LMR, ASME Code NH[2], ASME Code Case N-201-4[3], BDB code[4], and RCC-MR code[5] have been developed and continuously being upgraded to reduce the conservatism contained in design rules. Many researchers have studied the methods of the creep-fatigue damage evaluation using the elastic analysis approach and the simplified inelastic analysis approach for LMFBR design[6]. However, there are actually few published research results applying this elevated temperature design rules accounting for the creep and stress-rupture effects to LMR structural design.

The main purposes of this paper are to design the reactor internal structures of KALIMER(Korea Advanced LIquid MEtal Reactor), which are subjecting to elevated temperature, using the ASME Code Case N-201-4, and clearly establish the design by analysis procedures accounting for the creep and stress-rupture effects in elevated temperature design.

The annulus type internal structure called as the baffle annulus in KALIMER, which is composed of the RV liner, the support barrel, the baffle plate, and the separation plate, is designed to mitigate the large thermal gradients generated between hot and cold sodium boundaries. The temperature of stagnant sodium in the baffle annulus is steadily stratified at all operating conditions and will greatly reduce the thermal stresses of boundary regions of hot and cold sodium[7].

In previous research works[8], brief evaluations of the structural integrity of the baffle annulus regions in KALIMER reactor internal structures have been carried out using the elastic analysis method provided in ASME Code Case N-201-4 to check the load-controlled quantities and the total accumulated inelastic strains. From this work, the load-controlled quantities satisfy the ASME code rules but the total inelastic strain accumulated during total service lifetime at the elevated temperature does not satisfy the rules of ASME Code Case N-201-4.

In this paper, the more detail evaluations of the time dependent stress and the total accumulated inelastic strain, and the creep-fatigue damages for the reactor internal structures of KALIMER are carried out in case of the normal operation using the rules of ASME Code Case N-201-4 for elevated temperature.

To obtain the thermal stresses in sensitive internal structure regions, the detail heat transfer analysis, including the reactor vessel, containment vessel, collector cylinder, and cover gas, is carried out using combined heat conduction, convection, and radiation for the open space and closed space. For the seismic OBE stresses in two horizontal and one vertical direction, the quasi-static stress analyses are performed for the maximum peak acceleration responses obtained from detail seismic response analysis[9].

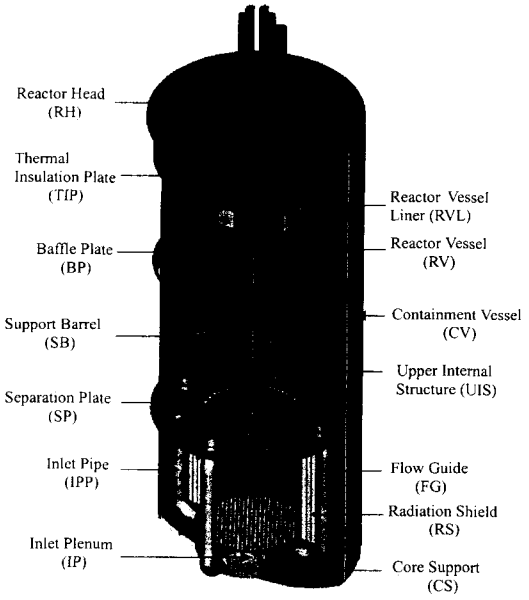

Fig. 1 Conceptually Designed KALIMER Reactor Internal Structures

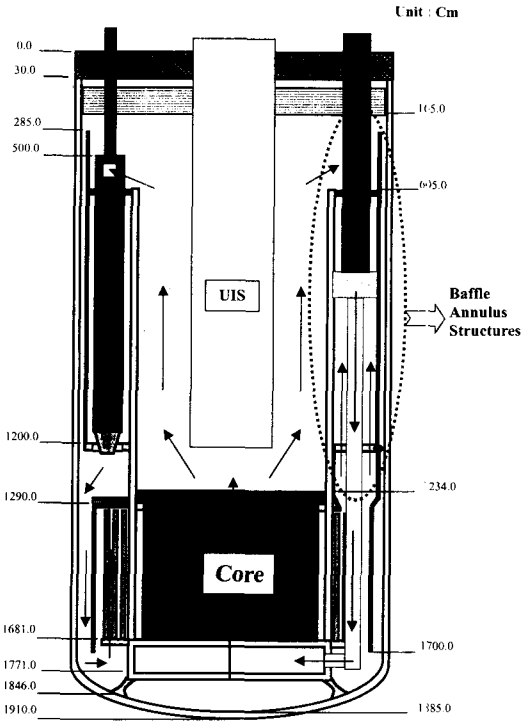

Fig. 2 Elevations of KALIMER Reactor Internal Structures

2. Main Design Features

The KALIMER reactor internal structures are composed of the Core Support Structure, the Inlet Plenum, the Support Barrel, the RV Liner, the Baffle Plate, the Separation Plate, the Flow Guide, the EMP Nozzle, the Inlet Pipe, and the Radiation Shield Structures. Fig. 1 shows the assembled reactor internal structures including the containment vessel, reactor vessel, reactor internal structures, and components.

KALIMER reactor internal structures have 3-main functions providing 1) core support, 2) primary coolant flow path, and 3) component support. Basically all reactor internal structures are designed to meet these functional requirements. The design basis of KALIMER reactor internal structures is preliminary described in Ref. [7].

Fig. 2 shows the elevations of each reactor structure part and Table 1 shows the dimension and material design data. As shown in figure and table, KALIMER reactor vessel is 17.0m height of side cylinder, 7.02m outer diameter, and 0.05m thickness. For the material data of the reactor internal structures, 304 SS or 316 SS will be used but these materials are studying to be replaced by 316 LN.

The general seismic design features of KALIMER reactor internal structures are the horizontally coupled between the fixed structures and the components at the baffle plate and the separation plate to remove the disadvantage of a single-stand cantilever structural type as shown in Fig. 2.

The annulus type internal structure called as the baffle annulus, which is composed of the RV liner, the support barrel, the baffle plate, and the separation plate, is provided to mitigate the large

Table 1. Dimensions of Conceptually Designed KALIMER Reactor Structures

Items	Outer Dia. (Cm)	Thickness (Cm)	Material	Remark (Cm)
1. Containment Vessel	737.0	2.5	2(1/4)Cr-1Mo	Partial-spherical bottom head
2. Reactor Vessel	702.0	5.0	316SS	Gap between RV and CV = 15.0
3. RV Liner	687.0	2.5	316SS	Gap between RVL and RV = 2.5
4. Support Barrel	374.0	5.0	316SS	Gap between SB and IHX = 16.925
5. Inlet Plenum	374.0	15.0	304SS	Upper Grid Plate T=10.0 Lower Grid Plate T=15.0
6. Baffle Plate	687.0	2.5	316SS	Lower Baffle Plate T=2.5 Upper Baffle Plate T=2.5
7. Separation Plate	687.0	10.0	316SS	Circular Disk Type
8. Core Support	374.0(t) 454.0(b)	15.0	316SS	Skirt Type, Height=60
9. Core	344.0	-	-	Gap between Core and SB = 10.0
10. Reactor Head	737.0	30.0	304SS	Circular Disk Type
11. Flow Guide	660.0	2.5	304SS	
12. Inlet Pipe	45.08	2.54	316SS	4 EA
13. Core Shield	248.0	15x3	316SS	3-Cylinder Type, Gap=3 Height=370
14. Former Ring	358.0	10.0	316SS	
15. EMP Nozzle	125.0	2.5	316SS	Height=80

* O.D. of IHX (4EA) = 120 cm
* O.D. of EM-Pump (4EA) = 120 cm
* T : Thickness
* t, b : top, bottom

>>> On material data, 316SS is studying to be replaced by 316LN.

thermal gradients generated between hot and cold sodium boundaries. The temperature of stagnant sodium in the baffle annulus is steadily stratified at all operating conditions and will greatly reduce the thermal stresses of boundary regions of hot and cold sodium.

3. Stress Calculations

3.1. Heat Transfer Analysis

As first step to calculate the thermal stresses, the heat transfer analysis is performed to obtain the thermal gradients of the metal for the bulk temperature of the sodium coolant flowing around the reactor internal structures as follows.

3.1.1. Analysis Model

Radial and axial thermal gradients of the reactor internal structures in the baffle annulus region, which includes the support barrel, the separation plate, the baffle plate, the reactor vessel liner, and flow guide, are calculated from the finite element analyses for the normal operation using an axisymmetric analysis model bounded by elevations 165cm and 1500cm in the axial direction. The elevation 165cm is the location of the bottom end of the thermal insulation plate. Fig.3 shows the schematic drawing of the heat

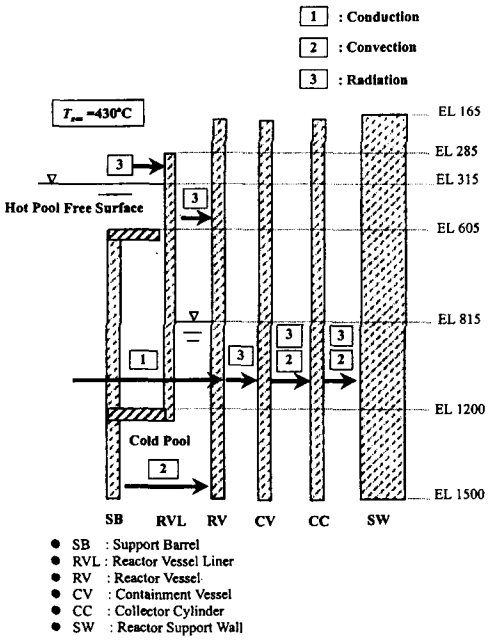

Fig. 3. Heat Transfer Mechanism Used in Analysis

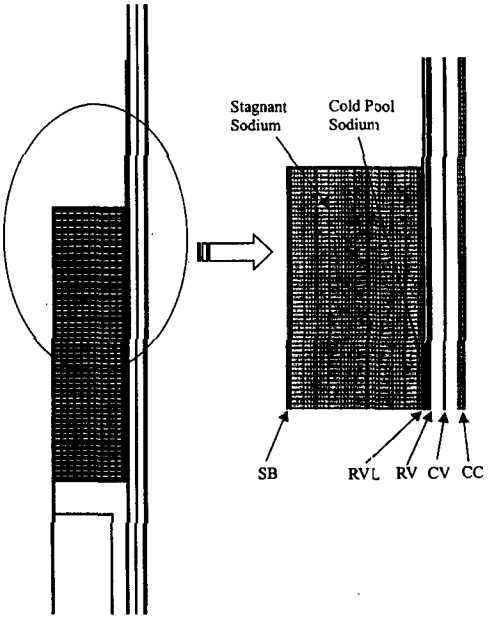

Fig. 4. Axisymmetric Finite Element Model of the Baffle Annulus of Reactor Internal Structures

transfer mechanism assumed in analysis. As shown in figure, the baffle annulus region of the internal structures presents a very complex heat transfer mechanism including the conduction, convection, and heat radiation. The convection heat transfer is applied to the support barrel inner surface, the baffle plate upper surface, the inner surface of the reactor vessel liner from the elevation of the baffle plate upper surface to the hot sodium free surface at elevation 315cm. The surfaces contacted to the cold pool region, which are the inner surface of the reactor vessel and outer surface of the support barrel from the elevations 1200cm to 1500cm and the flow guide surfaces have the convection heat transfer with the bulk temperature of the cold pool. Above the sodium free surfaces of the hot and cold pool, heat transfer across this region is by radiation only, as convection is assumed to be negligible. In this region, the radiation mechanism is assumed as the open system with the cover gas temperature 430°C. The conduction heat transfer occurs across the stagnant sodium inside of the baffle annulus structure to the reactor vessel liner. The conduction heat transfer also occurs between the reactor vessel liner and reactor vessel through the cold pool sodium inside of the annulus. The reactor vessel is thermally coupled to the containment vessel only by radiation heat transfer. Both convection and radiation are included in the analysis between the containment vessel and the PSDRS collector cylinder. The radiation between the reactor vessel and the containment vessel, and between the containment vessel and the PSDRS collector cylinder, is treated as the closed system.

Fig.4 shows an axisymmetric analysis model, which includes the reactor vessel, the containment vessel, and the PSDRS collector cylinder considering the heat transfer in the radial direction. The ANSYS 5.5 computer code[10] is

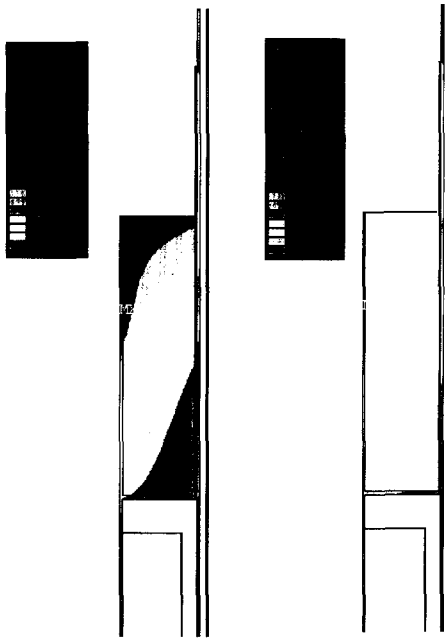

(a) Including Metal and Sodium (b) Only for Metal

Fig. 5. Temperature Distributions(Normal Operation)

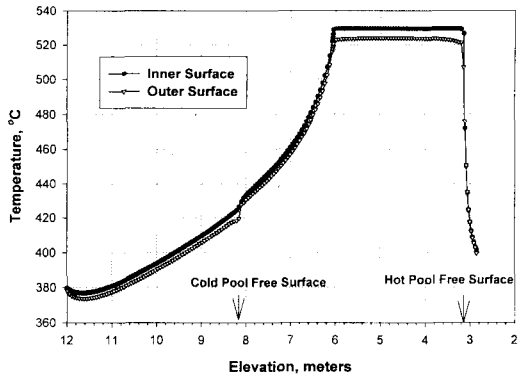

Fig. 6. Surface Temperatures of Support Barrel (Normal Operation)

used with STIFF 55 two-dimensional isoparametric thermal conduction and convection elements representing the structures and sodium, and with LINK32 element providing the 3-dimensional radiation links across structural gaps where no sodium is present. As shown in analysis model, the element size is enough to produce accurate results for radiation, which is so sensitive to element size. The thermal boundary conditions used in the thermal analysis are as follows:

a. The applied hot sodium bulk temperatures inside of the support barrel are 530℃ for upper region of the support barrel elevation and 430 ℃ for lower region of the support barrel elevation.
b. The cold sodium bulk temperature is 386℃, which is applied to the inner and outer surfaces of the flow guide, the bottom surface of the separation plate, the outer surface of the support barrel and the inner surface of the reactor vessel cylinder under the elevation of the separation plate.
c. The sodium bulk temperature in the annulus between the reactor vessel and the reactor vessel liner at elevation 1210cm is 386 ℃ with a film coefficient of 10^4 kg/hr.m^2.℃.
d. The boundary temperature of the outer surface of the collector cylinder is 30℃ over its entire length.
e. The bulk temperature of the air flowing through the annulus between the containment vessel and the collector cylinder is 85℃ with a film coefficient of 2.278 W/m^2.℃.
f. The temperatures of the reactor vessel at both the inner and outer surface at elevation 165cm are 350 ℃, which is calculated from COMMIX computer code.

3.1.2. Results of Thermal Analyses

Fig.5 shows the calculated temperature distributions of whole baffle annulus strcuture including the metal and the sodium for the normal operation. From the results, the stagnant sodium inside of the baffle annulus structure has a good function to make a stratified temperature distribution, which results in a significant reduction of the thermal gradient and heat loss. And the

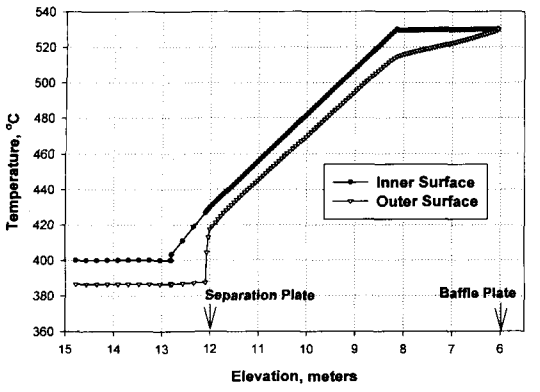

Fig. 7. Surface Temperature of RV Liner (Normal Operation)

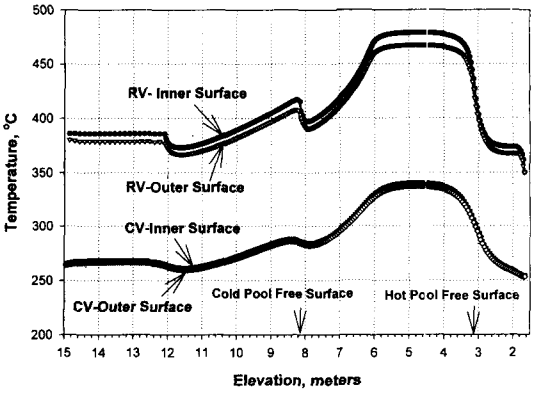

Fig. 8. Reactor and Containment Vessel Surface Temperature (Normal Operation)

large pressure drop in cold pool region inducing about 500cm elevation difference between the hot pool free surface and the cold pool free surface makes the surface temperature of the reactor vessel cylinder to be not in elevated temperature conditions.

The surface temperatures of the support barrel calculated from the ANSYS analysis are shown in Fig.6. The temperatures of the inner surface are the sodium pool temperatures specified as the boundary conditions of the analysis. A sharp radial and axial thermal gradient occurs at the junction region between the support barrel and the separation plate because the inner surface is contacted to the hot sodium and the outer surface of the support barrel and the separation plate bottom surface are contacted to the cold sodium.

The temperature variation in the reactor vessel liner surface from the ANSYS analysis is shown in Fig.7. At the inner surface, between elevation 315cm and 605cm, the temperatures are the hot sodium pool temperatures specified as the boundary conditions of the analysis. Above elevation 315cm, the liner receives heat energy by conduction from its lower elevation part and by radiation from the hot sodium pool, while losing the heat energy by radiation to the reactor vessel. This causes a sharp axial thermal gradient as well as a significant radial thermal gradient at elevation 315cm(Hot pool free surface). Large axial thermal gradients in the reactor vessel liner occur at elevations between 605cm and 1200cm reflecting the effect of the stagnant sodium inside of the baffle annulus structure. This means that the designed baffle annulus structure has a good function to produce a well-stratified temperature distribution between the hot sodium pool and the cold sodium pool. However, a large change in the axial thermal gradient occurs at the elevation of the cold pool free surface in the reactor vessel liner and the reactor vessel.

The surface temperature distributions in the reactor and containment vessel are shown in Fig.8. The trend of the temperature distributions along the axial direction are same in both vessels for normal operation. The most severe axial and radial thermal gradients of vessels occur at the elevation of the cold pool and hot pool free surfaces. In the annulus region filled with cover gas, the inner surface of the reactor vessel from the baffle plate 605cm to the hot pool free surface 315cm is greatly heated by radiation from the hotter reactor vessel liner and the reactor vessel outer surface radiates heat energy to the cooler

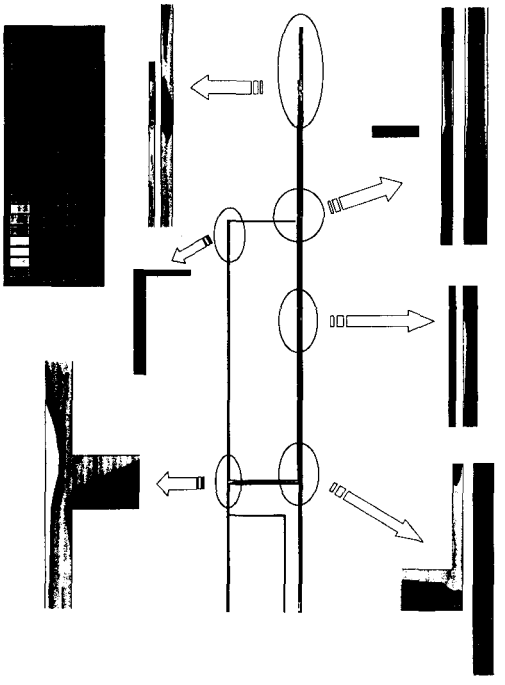

Fig. 9. Thermal Stress Distributions (Normal Operation)

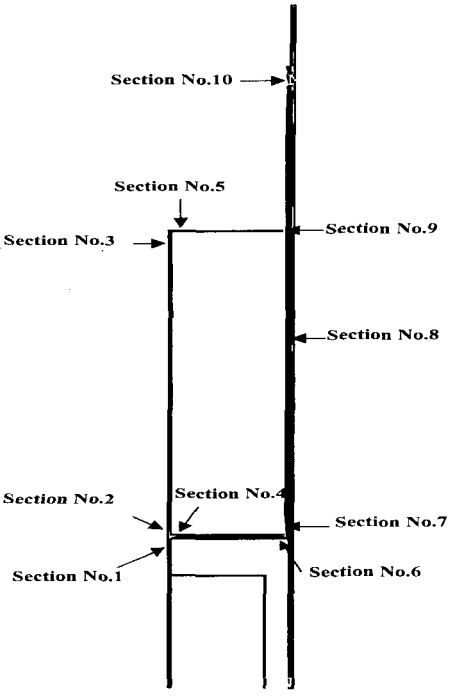

Fig. 10. Selected Sections Evaluating the Structural Integrity

containment inner surface, producing great radial thermal gradients as shown in Fig.8. As same as the reactor vessel liner, large axial thermal gradients occur in the reactor vessel at elevations from 815cm to 605cm by radiation with the reactor vessel liner and by conduction through the axial direction in the vessel. Above elevation 315cm, great axial thermal gradients occur in the reactor vessel. At normal operations, the maximum elevation difference between the hot pool free surface and the cold pool free surface is about 500cm brought by 5pa pressure drop. This makes the wall-averaged temperature of the reactor vessel cylinder at the cold pool free surface elevation to be under the elevated temperature regime.

3.1.3. Results of Thermal Stress Analyses

Fig. 9 shows the thermal stress distribution of the reactor internal structures for normal operation. As expected from the results of the thermal analysis for normal operation, the thermal stresses are significantly occurred at the junction part between the support barrel and the separation plate, and the junction part between the reactor vessel liner and the separation plate. And also large thermal stresses are occurred at the reactor vessel liner in the regions of the cold pool free surface region, the baffle plate elevation, and the hot pool free surface. Even high thermal stresses are occurred at the lower part of the support barrel below the separation plate elevation and the junction part between the reactor vessel liner and the separation plate, these parts are not experienced the elevated temperature during normal operation. Therefore, it is expected that there is no severe creep and ratcheting damage invoking the inelastic strain accumulation for the total service lifetime.

Table 2. Maximum Stress Intensities and Average Wall Temperature for Normal Operation

Section No. (Node-Node)	T_a (°C)	P_m	P_b	P_m+P_b	P_p	P_{total}
No. 1 (458-976)	404	34.7	69.9	103.6	1.0	103 6
No. 2 (481-993)	430	80.0	36.3	110.2	3.6	108 9
No. 3 (797-1239)	530	2.1	5.7	6.5	1.2	6.6
No. 4 (1332-1344)	400	10.7	27.9	35.0	1.4	34.0
No. 5 (2111-2474)	530	3.0	3.3	5.0	0.0	5.0
No. 6 (2502-2506)	386	28.3	22.7	50.6	12.3	57.4
No. 7 (2510-2748)	380	51.2	87.8	105.0	1.7	105 7
No. 8 (2509-2747)	430	6.5	11.1	17.5	0.4	17.4
No. 9 (2729-3077)	530	25.1	41.1	49.3	1.1	49.7
No.10 (3136-3086)	530	101.9	101.4	156.6	4.8	157.9

Table 3. Maximum Stress Intensities for OBE Load

Section No.	P_m	P_b	P_m+P_b	P_p	P_{total}
No. 1	16.9	18.4	25.6	0.8	25.4
No. 2	14.0	47.1	47.9	2.0	49.8
No. 3	1.7	4.8	5.0	0.31	5.3
No. 4	1.55	34.9	35.5	0.5	36.0
No. 5	1.7	32.9	33.8	0.1	33.8
No. 6	0.8	11.6	11.8	6.2	15.0
No. 7	14.4	51.8	53.9	0.8	54.6
No. 8	0.6	0.0	0.6	0.0	0.6
No. 9	0.3	0.0	0.3	0.0	0.3
No.10	0.03	0.0	0.03	0.0	0.03

From results of the thermal stress analysis, the critical sections for evaluating the structural integrity by ASME design code are selected as shown in Fig.10. Table 2 shows the maximum stress intensities and the wall-averaged temperatures for normal operation. In structural evaluations, the stresses caused by circumferential thermal gradients are assumed to be negligible.

3.2. Seismic Stresses for Operating Basis Earthquake (OBE)

To obtain the seismic stresses for OBE loads, the quasi-static analysis is performed for the maximum peak acceleration responses in horizontal direction, 0.075g, and vertical direction, 1.55g, obtained from detail seismic time history analysis[9]. Table 3 is the calculated maximum stress intensities for OBE load. From the results, it is shown that large seismic stresses are occurred at the junction part between the support barrel and the separation plate, and the junction part between the reactor vessel liner and the separation plate. The bending stress is dominant due to vertical seismic load.

Table 4. Maximum Stress Intensities for Dead Weight

Section No.	P_m	P_b	P_m+P_b	P_p	P_{total}
No. 1	10.9	11.9	16.5	0.5	16.4
No. 2	9.0	30.4	30.9	1.3	32.1
No. 3	1.1	3.1	3.2	0.2	3.4
No. 4	1.0	22.5	22.9	0.3	23.2
No. 5	1.1	21.2	21.8	0.08	21.8
No. 6	0.5	7.5	7.6	4.0	9.7
No. 7	9.3	33.4	34.8	0.5	35.2
No. 8	0.4	0.0	0.4	0.0	0.4
No. 9	0.2	0.0	0.2	0.0	0.2
No.10	0.02	0.0	0.02	0.0	0.02

3.3. Stresses for Dead Weight

The stresses for the dead weight are calculated to check the structural integrity of the design load. Table 4 shows the calculated maximum stress intensities occurring in sections of interest.

4. Structural Integrity Accounting for Creep and Stress-Rupture Effects

In this paper, ASME Code Case N-201-4[3] for elevated temperature design of reactor internal structures is used to evaluate the structural integrity of KALIMER reactor internal structures.

At temperatures and loading conditions where creep effects are significant, the design by analysis shall consider the time-dependent material properties and structural behavior by guarding against the failure modes such as the ductile rupture from short-term loadings, the creep rupture from long-term loadings, the creep-fatigue damage, the gross distortion due to incremental collapse and ratcheting. In evaluating the structural integrity for elevated temperature, it can be checked by four-quantities broadly such as 1) the load-controlled stress, 2) the total accumulated inelastic strain, 3) creep-fatigue damage, and 4) buckling instability. These are evaluated through following sections. Among these quantities, the buckling instability for the KALIMER reactor vessel has been already evaluated in Ref.[11].

4.1. Design Rules and Limits for Load-Controlled Stresses for Service Level A and B

The stress calculations required for the analysis of Level A and B Service Loadings are based on a linearly-elastic material model.

The calculated stress intensity values calculated in range of elevated temperature shall satisfy the following conditions.

Primary-Membrane Stress Intensity:

$$P_m \leq S_{mt} \tag{1}$$

Primary-Membrane Plus Bending Stress Intensity:

$$P_m + P_b \leq KS_m \tag{2}$$

$$P_m + P_b / K_t \leq S_t \tag{3}$$

From Eq.(1) to Eq.(3), S_{mt} is determined for the time, t, corresponding to the total duration of the particular loading during the entire service life, and for temperature, T, corresponding to the

Table 5. Service Limit Check for Load-Controlled Quantities When T_a < 427℃

Section No	Average Wall Temp. T_a (℃)	Check 1 ($P_m \leq S_m$)		Check 2 ($P_m + P_b \leq 1.5S_m$)		Check 3 ($P_m + P_b + Q \leq 3S_m$)	
		P_m	S_m	$P_m + P_b$	$1.5S_m$	$P_m + P_b + Q$	$3S_m$
No. 1	404	16.9	110.3	25.6	165.4	129.2	330.9
No. 2	430	-	-	-	-	-	-
No. 3	530	-	-	-	-	-	-
No. 4	400	1.55	110.3	35.5	165.4	70.5	330.9
No. 5	530	-	-	-	-	-	-
No. 6	386	0.8	111.7	11.8	167.5	62.4	335.1
No. 7	380	14.4	111.7	53.9	167.5	158.9	335.1
No. 8	430	-	-	-	-	-	-
No. 9	530	-	-	-	-	-	-
No.10	530	-	-	-	-	-	-

Table 6. Service Limit Check for Load-Controlled Quantities for Base Metal When $T_a \geq$ 427°C

Section No	Average Wall Temp. T_a (℃)	Check 1 ($P_m \leq S_{mt}$)		Check 2 ($P_m + P_b \leq KS_m$)		Check 3 ($P_m + P_b/K_t \leq S_t$)	
		P_m	S_{mt}	$P_m + P_b$	KS_m	$P_m + P_b/K_t$	S_t
No. 1	404	-	-	-	-	-	-
No. 2	430	14.0	109.0	47.9	163.3	51.7	141.3
No. 3	530	1.7	103.4	5.0	160.0	5.54	103.4
No. 4	400	-	-	-	-	-	-
No. 5	530	1.7	103.4	33.8	160.0	28.02	103.4
No. 6	386	-	-	-	-	-	-
No. 7	380	-	-	-	-	-	-
No. 8	430	0.6	109.0	0.6	163.3	0.6	141.3
No. 9	530	0.3	103.4	0.3	160.0	0.3	103.4
No10	530	0.03	103.4	0.03	160.0	0.03	103.4

maximum wall-averaged temperature that occurs during the particular loading event. S_t is a temperature and time-dependent stress intensity limit.

The factor K_t accounts for the reduction in extreme fiber bending stress due to the effect of creep. The factor is given by the following:

$$K_t = (K + 1) / 2 \quad (4)$$

The factor K, is the section factor for the cross section being considered. It is the ratio of the load set producing a fully plastic section to a load set producing initial yielding of the extreme fiber of the cross section. In evaluating across-the-wall bending of shell type structures, K=1.5 (for rectangular section) shall be used. Thus, for across-the-wall shell bending, K_t is 1.25 in Eq.(4).

The total service life of KALIMER reactor

Table 7. Service Limit Check for Load-Controlled Quantities for Weldments When $T_a \geq 427℃$

Section No	Average Wall Temp. T_a (℃)	Check 1 ($P_m \leq S_{mt}$) P_m	Check 1 $S'_{mt} = Min[S_m, 0.8S_r \cdot R]$	Check 2 ($P_m + P_b \leq KS_m$) $P_m + P_b$	Check 2 KS_m	Check 3 ($P_m + P_b/K_t \leq S_t$) $P_m + P_b/K_t$	Check 3 $S'_t = Min[S_t, 0.8S_r \cdot R]$
No. 1	404	-	-	-	-	-	-
No. 2	430	14.0	Min[109.0, 310.6]	47.9	163.3	51.7	Min[141.3,310.6]
No. 3	530	1.7	Min[103.4, 67.2]	5.0	160.0	5.54	Min[103.4, 67.2]
No. 4	400	-	-	-	-	-	-
No. 5	530	1.7	Min[103.4, 67.2]	33.8	160.0	28.02	Min[103.4, 67.2]
No. 6	386	-	-	-	-	-	-
No. 7	380	-	-	-	-	-	-
No. 8	430	0.6	Min[109.0, 310.6]	0.6	163.3	0.6	Min[141.3, 310.0]
No. 9	530	0.3	Min[103.4, 67.2]	0.3	160.0	0.3	Min[103.4, 67.2]
No.10	530	0.03	Min[103.4, 67.2]	0.03	160.0	0.03	Min[103.4, 67.2]

internal structures is 30 years(262.8×10^3hrs). The wall-averaged temperatures of each section being evaluated are shown in Table 2.

Table 5 shows the results of the service limit check for load-controlled quantities when $T_a <$ 427℃. For the sections of $T_a <$ 427℃, i.e., not elevated temperature, the rules of NG-3220[8] is applied. The stresses of these sections satisfy the design rules with enough margins. Table 6 and Table 7 are the evaluation results for the sections of elevated temperature($T_a \geq$ 427℃) when all sections are assumed as the base metal and the weldment respectively. From the results, all sections evaluating the service limits for the Service Level A and B satisfy the rules of load-controlled service limits for any cases of the base metal and the weldment.

4.2. Deformation and Strain Limits for Structural Integrity

4.2.1. Limits for Inelastic Strains

In regions expecting elevated temperatures the maximum accumulated inelastic strain shall not exceed the following values.

(a) Strains averaged through the thickness, 1% : *Membrance* $\varepsilon_m \leq$ 1.0%

(b) Strains at the surface, due to an equivalent linear distribution of strain through the thickness, 2% : *Bending* $\varepsilon_b \leq$ 2.0%

(c) Local strains at any point, 5% : Local $\varepsilon_L \leq$ 5.0%

4.2.2. Using Elastic Analysis Method

The strain limits of Y-1310 are considered to have been satisfied if the limits of any one of Test No. A-1, Test No. A-2, or Test No. A-3 are satisfied.

To establish the appropriate cycle to be evaluated in Test Nos. A-1 and A-2, an individual cycle, as defined in the DS(Design Specification) can not be split into subcycles to satisfy these requirements because the maximum range of the secondary stress intensity during the cycle may not be selected in the split subcycles. And at least one cycle must be defined that includes the maximum

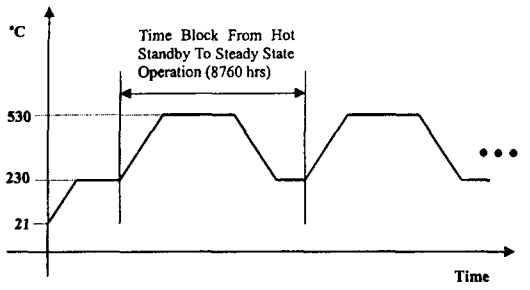

Fig. 11. Assumed Normal Operation Cycles in Structural Evaluation

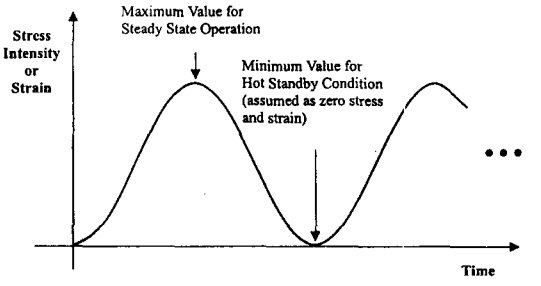

Fig. 12. Assumed Stress Level for Normal Operation

Table 8. Service Limit Check for Deformation-Controlled Quantities

Section No	Test No. A-1 ($X+Y \le S_a / S_y$)				
	$X+Y$	S_y	S_a = Min[$1.25S_t \mid_{t=10^4\,hr}$, S_y]	S_a / S_y	Satisfaction
No. 1	-	-	-	-	-
No. 2	0.393 + 0.838=1.231	131.5	131.5	1	No
No. 3	0.043 + 0.050=0.093	129.8	129.8	1	Yes
No. 4	-	-	-	-	-
No. 5	0.216 + 0.039=0.254	129.8	129.8	1	Yes
No. 6	-	-	-	-	-
No. 7	-	-	-	-	-
No. 8	0.005 + 0.133=0.138	131.5	131.5	1	Yes
No. 9	0.002 + 0.380=0.382	129.8	129.8	1	Yes
No.10	0.000 + 1.206= 1.206	129.8	129.8	1	No

value of $(P_m + P_b/K_t)$ which occur during all level A, B, and C Service Loadings.

The stress indices to be used in Test Nos. A-1 and A-2 are defined as follows:

$$X \equiv (P_m+P_b/K_t)_{max} \div S_y,\ Y \equiv (Q_R)_{max} \div S_y \qquad (5, 6)$$

Note that S_y is the average of the S_y values at the maximum and minimum wall-averaged temperatures during the cycle being evaluated. The value of $(Q_R)_{max}$ is the maximum range of the secondary stress intensity during the cycle being considered.

The thermal loading cycle considered in evaluation is the normal operation having the process of the hot standby condition(230℃)-the steady state(530℃)-the hot standby condition (230 ℃) as shown in Fig.11. For this cyclic operation, it is assumed that the heat-up and cool-down process is so slow and taking long time enough to mitigate the peak stress increment and the stress fields in conditions of the hot standby are free. Therefore, the maximum range of the secondary stress intensity $(Q_R)_{max}$ is assumed as the maximum secondary stress intensity obtained from the steady state condition conservatively as shown in Fig.12.

The intent of this stress cycle is to demonstrate the adequacy of the design with conservative assumptions whenever possible.

Test No. A-1

$$X + Y \leq S_a / S_y \tag{7}$$

where S_a = Min[$1.25S_t|_{t=10^4 hrs}$, S_y]. Table 8 is the evaluation results of the deformation and strain limits for structural integrity using the Test No. A-1. In this evaluation, the support barrel near upper junction part with the separation plate(section no.2) and the reactor vessel liner of hot pool free surface region(section no.10) do not satisfy the deformation and strain limit rules.

Test No. A-2

$$X + Y \leq 1 \tag{8}$$

This is for those cycles during which the average wall temperature at one of the stress extremes defining the maximum secondary stress range $(Q_R)_{max}$ is below the applicable temperature in ASME Code Case N-201-4. For material Type 316SS, the applicable temperature at which $S_m=S_t|10^5$ is 544℃(1011°F). Then, the maximum average wall temperature for normal operation is 530℃ and it can be applicable for this Test A-2. However, the condition of Test No A-2 is same as the Test No. A-1 with $S_a/S_y=1.0$, therefore the evaluation results are same as Table 8.

Test No. A-3

For Test No. A-3, the limits of NG-32222.2, NG-3222.3, and NG-3222.5 shall be met and, in addition, the requirements of (a) through (e) below shall be satisfied.

(a) Sum of the Use-Fractions

$$\sum_i t_i / t_{id} \leq 0.1 \tag{9}$$

where t_i is the total duration of time during the service lifetime that the metal is at temperature, T_i and t_{id} is the maximum allowable time as determined by the stress-to-rupture value at temperature T_i and a stress value of $1.5S_y|_{Ti}$. Total duration of time t_i, during the service lifetime that the metal is at temperature, T_i, is 2.628×10^5 hours. The sections with elevated temperatures of 430℃ and 530℃ are evaluated as

For Sections with T_i =430℃:

$$1.5S_y|_{Ti=430} = 180.9\text{MPa}, \; t_{id}=5.0\times10^6 \text{ hrs}$$

$$\sum_i t_i / t_{id} = 0.053 < 0.1 \text{ (Satisfy)}$$

For Sections with T_i =530℃:

$$1.5S_y|_{Ti=530} = 175.8\text{MPa}, \; t_{id}=2.0\times10^4 \text{ hrs}$$

$$\sum_i t_i / t_{id} = 13.14 > 0.1 \text{ (Not satisfy)}$$

From above results, the sum of the use-fractions is satisfied for the sections operated at T_i =430℃ but not at T_i =530℃ during normal operation with the total service lifetime. To satisfy this rule for the hold temperature T_i =530℃, the total duration at this temperature should be limited under 2000 hours.

(b) Creep Strains

$$\sum_i \varepsilon_i \leq 0.2\% \tag{10}$$

where ε_i is the creep strain that would be expected from a stress level of $1.25S_y|_{Ti}$ applied for the total duration of time during the service lifetime that the metal is at T_i. With using the isochronous stress-strain curves[3], the total creep strain for the total service lifetime at T_i can be obtained as follows;

Table 9. Results of S_m Limits Without Explicit Consideration of Creep and Stress-Rupture

Section No	Average Wall Temp. T_a (°C)	Test No. A-3 ($P_m+P_b+Q \le 3S_m$ or $3\bar{S}_m$)			
		P_m+P_b+Q	$3S'_m$	$3S'_m=Min[3S_m, 3\bar{S}_m=(1.5S_m+S_{rH})]$	Satisfaction
No. 1	404	129.2	330.9	-	Yes
No. 2	430	158.1	-	Min[326.8, 301.3]	Yes
No. 3	530	11.5	-	Min[318.5, 186.8]	Yes
No. 4	400	70.5	330.9	-	Yes
No. 5	530	38.8	-	Min[318.5, 186.8]	Yes
No. 6	386	62.4	335.1	-	Yes
No. 7	380	158.9	335.1	-	Yes
No. 8	430	18.1	-	Min[326.8, 301.3]	Yes
No. 9	530	49.6	-	Min[318.5, 186.8]	Yes
No.10	530	156.6	-	Min[318.5, 186.8]	Yes

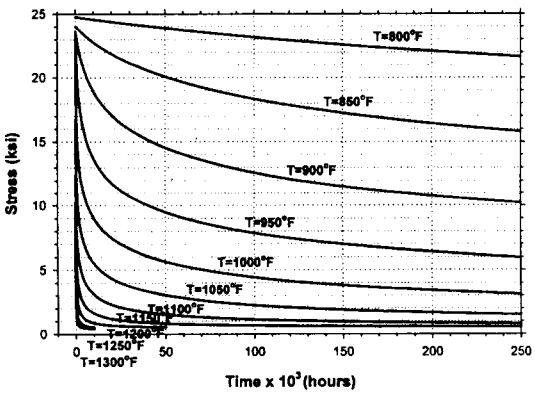

Fig. 13. Calculated Stress Relaxation Strength (316SS)

For Sections with T_i =430°C:

Creep strain, ε_i | $_{1.25S_y|Ti=150.8MPa}$

= 0.3% (Not satisfy)

For Sections with Ti=530°C:

Creep strain, ε_i | $_{1.25S_y|Ti=146.5MPa}$

= 0.7% (Not satisfy)

In these results, this rule is very conservative when the isochronous stress-strain curve is used for calculating the creep strain expected from a stress level of $1.25S_y$ | $_{Ti}$.

(c) $3S_m$ Limits

For the $3S_m$ limit in NG-3222.2 and NG-3222.3 of ASME Code Subsection NG, the modified $3S'_m$ values shall be used as follow:

When only one extreme of the stress difference occurs at the elevated temperature:

$$3\bar{S}_m = (1.5S_m + S_{rH}) \quad (11)$$

When both extremes of the stress difference occurs at the elevated temperature:

$$3\bar{S}_m = (1.5S_m + S_{rH}) \quad (12)$$

where S_{rH} and S_{rL} are the relaxation strengths associated with the temperatures at the hot and cold extremes of the stress cycle. These relaxation strengths may be determined by performing a pure uniaxial relaxation analysis starting with a initial stress of $1.5S_m$ and holding the initial strain throughout the time interval equal to the time of service above 427°C.

The creep equations used in the uniaxial relaxation analysis are presented in Appendix-A. Fig.13 is the calculated relaxation strengths for

316SS material with the metal temperature variations. As shown in the calculated relaxation strength of 316SS, the relaxation strengths decrease significantly as increase the metal temperature.

Table 9 is the results of evaluation and it is shown that all sections of interest satisfy the $3S_m$ limits without explicit consideration of creep and stress-rupture.

4.2.3. Using Simplified Inelastic Analysis

The limits for inelastic strains are considered to have been satisfied if the limits of any one of the following Test No.B-1, Test No.B-2 or Test No.B-3 are satisfied.

Test No.B-1 can be used only for the axisymmetric structures subjected to axisymmetric loadings and away from local structural discontinuities, or general structures in which the peak through-the-wall thermal stress is negligible (i.e., the thermal stress distribution is linear through the wall). Test No.B-2, which is more conservative, is applicable to any structure and loadings. Test No.B-3 may be used for cycles in regimes R_1 and R_2 in Fig.Y-1330-1. This procedure may also be applied to cycles in the S_1, S_2, and P regimes in order to minimize the conservatism in calculated strains when there are a few relatively severe cycles.

Note that in calculating the primary stress index X, the secondary stresses with elastic followup (i.e., pressure-induced membrane and bending stresses and thermal-induced membrane stresses) are classified as primary stresses for purposes of this evaluation. In calculating the X and Y, the S_{yL} value shall be used instead of S_y for Test Nos, B-1 and B-2.

Test No. B-1 and B-2

The elastically calculated primary and secondary stress intensities are used to determine an effective creep stress

$$\sigma_c = Z \cdot S_{yL} \tag{13}$$

which in turn is used to determine a total ratcheting creep strain. The dimensionless effective creep stress parameter Z for any combination of loading, which is determined by the calculated stress indices X and Y, is given in Fig. Y-1330-1 for Test No. B-1 and in Fig. Y-1330-2 for Test No. B-2 of Ref[3].

The creep-ratcheting strain is determined by multiplying σ_c by 1.25 and evaluating the creep

Table 10. Calculated Effective Creep Stress for Elevated Temperature Sections (Test No. B-1)

Section No	Effective Creep Stress (Test No. B-1)						
	X	Y	Z	S_{yL}	S_{yH}	$\sigma_c = Z \cdot S_{yL}$	Check of $\sigma_c \leq S_{yH}$
No. 1	-	-		-	-	-	-
No. 2	0.92	0.25	0.90	142.4	120.6	128.2	No
No. 3	0.05	0.04	0.05	142.4	117.2	7.1	Yes
No. 4	-	-		-	-	-	-
No. 5	0.22	0.02	0.22	142.4	117.2	31.3	Yes
No. 6	-	-		-	-	-	-
No. 7	-	-		-	-	-	-
No. 8	0.05	0.08	0.05	142.4	120.6	7.1	Yes
No. 9	0.17	0.33	0.17	142.4	117.2	24.2	Yes
No.10	0.72	0.71	0.75	142.4	117.2	106.8	Yes

Table 11. Service Limit Check for Total Inelastic Strain (Test No. B-1)

Section No	Test No. B-1					
	$1.25\sigma_c$ (MP_a)	Total Creep-Ratcheting Strain, $\Sigma \varepsilon_t$ (%)	Limit for Parent Metal		Limit for Weld Metal	
No. 1	-	-	-	-	-	-
No. 2	160.25	0.55	1.0	OK	0.5	Not OK
No. 3	8.88	0.00	1.0	OK	0.5	OK
No. 4	-	-	-	-	-	-
No. 5	39.13	0.03	1.0	OK	0.5	OK
No. 6	-	-	-	-	-	-
No. 7	-	-	-	-	-	-
No. 8	8.88	0.00	1.0	OK	0.5	OK
No. 9	30.25	0.025	1.0	OK	0.5	OK
No.10	133.5	0.90	1.0	OK	0.5	Not OK

Table 12. Calculated Effective Creep Stress for Elevated Temperature Sections (Test B-2)

Section No	*Effective Creep Stress (Test No. B-1)*					
	X	Y	Z	S_{yL}	S_{yH}	$\sigma_c = Z \cdot S_{yL}$
No. 1	-	-	-	-	-	-
No. 2	0.92	0.25	1.0	142.4	120.6	142.4
No. 3	0.05	0.04	0.1	142.4	117.2	14.24
No. 4	-	-	-	-	-	-
No. 5	0.22	0.02	0.3	142.4	117.2	42.72
No. 6	-	-	-	-	-	-
No. 7	-	-	-	-	-	-
No. 8	0.05	0.08	0.1	142.4	120.6	14.24
No. 9	0.17	0.33	0.25	142.4	117.2	35.60
No.10	0.72	0.71	0.9	142.4	117.2	128.16

strain associated with the $1.25\sigma_c$ stress held constant throughout the temperature-time history of the entire service life. The isochronous stress-strain curves of Ref[3] shall be used to obtain the creep-ratcheting strain. The total creep-ratcheting strain shall be limited to 1% for parent metal and 1/2% for weld metal.

Table 10 shows the calculated effective creep stresses for Test No. B-1. To use Test No. B-1, the creep stress, σ_c, shall be less than the yield stress of S_{yH}, but the section no.2 is not met this rule. For the section no.2, the dimensionless effective creep stress parameter Z is not within the regimes E, S_1, S_2, and P in Fig. Y-1330-1 of Ref[3], so it is out of valid range of Test No. B-1. However, the section no.2 can be evaluated by the Test No. B-3.

Table 11 is the results of the service limit check of the total inelastic strain by using Test No. B-1. All sections of interest satisfy the rule of 1% strain when all sections are assumed as parent metal.

Table 13. Service Limit Check for Total Inelastic Strain (Test No. B-2)

Section No	Test No. B-1					
	$1.25\sigma_c$ (MP_a)	Total Creep-Ratcheting Strain, $\Sigma\varepsilon_t$ (%)	Limit for Parent Metal		Limit for Weld Metal	
No. 1	-	-	-	-	-	-
No. 2	178.00	1.20	1.0	Not OK	0.5	Not OK
No. 3	17.80	0.01	1.0	OK	0.5	OK
No. 4	-	-	-	-	-	-
No. 5	53.40	0.05	1.0	OK	0.5	OK
No. 6	-	-	-	-	-	-
No. 7	-	-	-	-	-	-
No. 8	17.80	0.01	1.0	OK	0.5	OK
No. 9	44.50	0.03	1.0	OK	0.5	OK
No.10	160.20	2.40	1.0	Not OK	0.5	Not OK

Table 14. Calculated Effective Creep Stresses for Test No. B-3

Section No.	T_a	E_L	E_H	X_L, X_H	Y_L, Y_H	Z_L, Z_H	σ_{cL}	σ_{cH}
No. 2	430	180.0	166.0	0.92, 0.66	0.25, 0.30	0.90, 0.66	128.2	158.78

Even though all sections are assumed as weldment parts, this rule is satisfied except of the section no.10(the part of reactor vessel liner at hot pool free surface). Actually, this part is not weldments.

Table 12 is the calculated effective creep stresses for Test No. B-2 and Table 13 is the results of the service limit check of the total inelastic strain. From the results, the section nos.2 and 3 do not satisfy this rule, therefore it is shown that Test No. B-2 gives more conservative results of the total creep-ratcheting strain than Test No. B-1.

Test No. B-3

As an alternate to the use of Test No. B-1 and B-2, the inelastic strains due to any number of selected operational cycles (i.e., relatively severe cycles in regimes R_1 and R_2) may be evaluated separately by Test No. B-3 or using detailed inelastic analysis in order to minimize the conservatism in the calculated strains. This method is applicable only to axisymmetric structures subjected to axisymmetric loadings and away from local structural discontinuities.

The total inelastic strains accumulated in the lifetime of the component are given by:

$$\sum\varepsilon_t = \sum\nu + \sum\eta + \sum\delta \tag{14}$$

Each component of Eq.(14) is obtained from the followings.

Σ_ν = the inelastic strains obtained from the isochronous curves in Test No. B-1

Σ_η = the plastic ratchet strain increments occurring for only $[\sigma_{cL}] \geq S_{yH}$

Table.15. Service Limit Check for Total Inelastic Strain (Test No. B-3)

Test No. B-3								
Section No	Inelastic Strain From Fig.Y-1800 $\Sigma\nu$	Plastic Ratchet Strain $\Sigma\eta$	Enhanced Creep Strain $\Sigma\delta$	Total Inelastic Strain, $\Sigma\epsilon_t$(%)	Limit for Parent Metal		Limit for Weld Metal	
No. 2	0.00	0.40	0.0	0.4	1.0	OK	0.5	OK

$$= \frac{1}{E_H}\left[([\sigma_{cL}] - S_{yH}) + ([\sigma_{cH}] - S_{yL})\right] \quad (15)$$

for $Z_L \le 1.0$

$$= \frac{1}{E_L}([\sigma_{cL}] - S_{yL}) + \frac{1}{E_H}([\sigma_{cH}] - S_{yH}) \quad (16)$$

for $Z_L > 1.0$

where $[\sigma_{cL}]$ and $[\sigma_{cH}]$ are the effective stresses for cold and hot extremes of the cycles as given by $[\sigma_{cL}] = Z_L S_{yL}$ and $[\sigma_{cH}] = Z_H S_{yH}$ respectively.

$\Sigma\delta$ = the enhanced creep strain increments due to stress relaxation

$$= \frac{1}{E_H}\frac{S_{yH}^2 - \sigma_c^2}{\sigma_c} \quad \text{for cycles where } [\sigma_{cL}] \ge S_{yH} \quad (17)$$

$$= \frac{1}{E_H}\frac{[\sigma_{cL}]^2 - \sigma_c^2}{\sigma_c} \quad \text{for cycles where } [\sigma_{cL}] < S_{yH} \quad (18)$$

where σ_c is the effective creep stress. All values in equations of the enhanced creep strain are related to the load cycle (n). And only positive $\delta_{(n)}$ increments should be considered.

For the section no. 2 of interest, the dimensionless effective creep stress parameter Z is within the regimes R_1 and R_2 as shown in Table 10, therefore, this Test No. B-3 can be used to check the total inelastic strain. For this purpose, it is assumed that there is no previous stress cycles, so that no accumulated inelastic strain obtained from the isochronous curves as in Test No. B-1 ignoring the increase of σ_c stress for cycles evaluated using Test No. B-3 because the cyclic normal operation itself is assumed as severe cycle for the section no.2. Therefore, $\Sigma\nu$ and $\Sigma\delta$ in Eq.14 are assumed as zero.

Table 14 is the calculated effective creep stress at the section no. 2 for using Test No. B-3. From this results, it is valid to calculate the plastic ratchet strain increments, $\Sigma\eta$, because $[\sigma_{cL}]$ =128.2 MPa is greater than S_{yH} = 120.6 MPa. According as Z_L < 1.0, $\Sigma\eta$ can be calculated using the Eq.(15).With considering the cycles, n=30, of the normal operation assumed in this evaluation, the calculated plastic ratchet strain increments, $\Sigma\eta$, is 0.4%. Therefore, as shown in Table 15, the section no.2 satisfies the rules of total inelastic strain limit when using the Test No. B-3.

4.3. Creep-Fatigue Evaluation at Elevated Temperatures

The accumulated creep and fatigue damage shall satisfy the following relation for the combination of Levels A, B, and C Service Loadings.

$$\sum_{j=1}^{p}\left(\frac{n}{N_d}\right)_j + \sum_{k=1}^{q}\left(\frac{\Delta t}{T_d}\right)_k \le D \quad (19)$$

where

D = total creep-fatigue damage

P = number of different cycle types

$(n)_j$ = number of applied repetitions of cycle type, j

$(N_d)_j$= number of design allowable cycles for cycle

Table 16. Maximum Value of Calculated Equivalent Strain Ranges (Normal Operation)

Node No		$\Delta\varepsilon_x \times 10^{-3}$	$\Delta\varepsilon_y \times 10^{-3}$	$\Delta\varepsilon_z \times 10^{-3}$	$\Delta\varepsilon_{xy} \times 10^{-3}$	$\Delta\varepsilon_{max} \times 10^{-3}$
Lower	458	0.31560	-0.20368	-0.49835	0.01212	0.549
SB/SP	976	-0.19167	0.31404	0.08838	-0.01130	0.482
Upper	481	0.12041	0.28790	-0.56018	0.06714	0.600
SB/SP	993	0.18707	-0.04557	-0.31861	0.09103	0.343
SB/BP	797	0.02405	-0.02362	-0.03078	0.00262	0.040
	1239	-0.16359	0.03039	0.00649	-0.00262	0.031
SP/SB	1332	-0.03540	-0.07418	0.09963	-0.00972	0.122
	1344	-0.10761	0.10150	-0.16458	0.00562	0.187
BP/SB	2111	-0.01996	0.01185	-0.00630	0.00004	0.021
	2474	0.01565	0.00429	-0.02586	-0.00009	0.033
SP/RVL	2502	0.00433	-0.03960	0.07688	0.03308	0.081
	2506	-0.19588	-0.01128	0.23790	-0.06514	0.293
RVL/SP	2510	0.15016	-0.54620	0.26138	-0.04516	0.584
	2748	-0.29405	0.35206	0.30291	-0.03253	0.480
RVL-Cold	2509	0.01470	-0.02677	-0.02107	0.00204	0.030
Free	2747	-0.03591	0.00421	0.10249	0.00255	0.095
RVL at BP	2729	0.17070	-0.16533	-0.24155	0.00486	0.292
Elev.	3077	-0.07976	0.26313	-0.08313	0.00686	0.265
RVL- Hot	3136	0.45305	-0.36914	-0.84765	-0.02960	0.877
Free	3086	-0.10031	0.73233	-0.47859	-0.03944	0.826

type, j

q = number of time intervals for the creep damage calculation

$(T_d)_k$ = allowable time duration determined from the stress-to-rupture curves

The total damage, D, shall not exceed the creep-fatigue damage envelope curves of Fig. 14.

4.3.1. Evaluation of Fatigue Damage

An equivalent strain range is used to evaluate the fatigue damage sum for both elastic and inelastic analysis. For evaluations of the fatigue damage, the wall-averaged temperatures of the section nos. 1, 4, 6 and 7 are assumed to be the lower bound of elevated temperature as 427℃ conservatively.

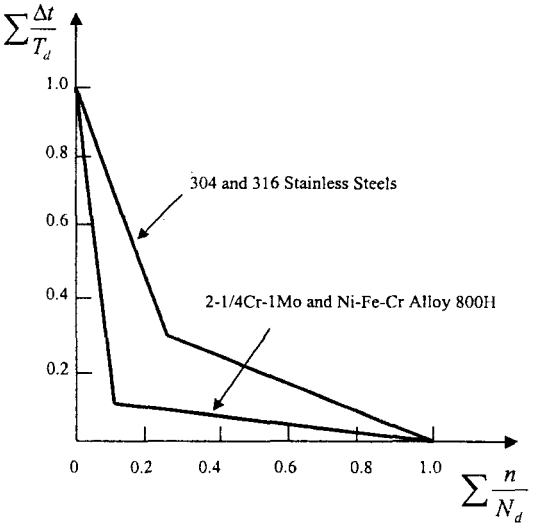

Fig. 14. Creep-Fatique Damage Envelop Curves

The equivalent strain for each point in time shall be calculated as:

Table 17. Calculated Parameters for Modified Equivalent Strain Range(Normal Operation)

Node No	$\Delta\varepsilon_{max} \times 10^{-3}$	S_{rH}	S^*	$\overline{S}$	K	K_e
458	0.549	151.7	242.5	243.4	1.010	1.0
976	0.482	151.7	231.5	232.2	1.010	1.0
481	0.600	124.1	220.6	223.8	1.033	1.0
993	0.343	124.1	179.2	181.1	1.033	1.0
797	0.040	20.7	28.4	29.8	1.185	1.0
1239	0.031	20.7	26.7	27.7	1.185	1.0
1332	0.122	151.7	171.8	172.6	1.040	1.0
1344	0.187	151.7	182.6	183.8	1.040	1.0
2111	0.021	20.7	23.0	23.0	1.000	1.0
2474	0.033	20.7	24.3	24.3	1.000	1.0
2502	0.081	151.7	165.1	168.3	1.243	1.0
2506	0.293	151.7	200.2	211.9	1.243	1.0
2510	0.584	151.7	248.3	249.8	1.016	1.0
2748	0.480	151.7	231.1	232.3	1.016	1.0
2509	0.030	124.1	128.9	129.0	1.023	1.0
2747	0.095	124.1	139.3	139.7	1.023	1.0
2729	0.292	20.7	77.0	78.3	1.022	1.0
3077	0.265	20.7	71.8	73.0	1.022	1.0
3136	0.877	20.7	144.8	148.3	1.031	1.0
3086	0.826	20.7	143.4	146.2	1.031	1.0

$$\Delta\varepsilon_{equiv,i} = \frac{\sqrt{2}}{2(1+\nu^*)}[(\Delta\varepsilon_{xi}-\Delta\varepsilon_{yi})^2+(\Delta\varepsilon_{yi}-\Delta\varepsilon_{zi})^2+(\Delta\varepsilon_{zi}-\Delta\varepsilon_{xi})^2+\frac{3}{2}(\Delta\gamma_{xyi}^2+\Delta\gamma_{yzi}^2+\Delta\gamma_{zxi}^2)]^{1/2} \quad (20)$$

where $\nu^* = 0.3$ when using the elastic analysis and $\nu^* = 0.5$ when using the inelastic analysis.

The maximum values of the calculated equivalent strain ranges, $\Delta\varepsilon_{max}$, for the thermal load of the normal operation are shown in Table 16. Note that the strain components to be used in calculating $\Delta\varepsilon_{max}$ do not include the local geometric stress concentration effects. Therefore, the modified maximum equivalent strain range $\Delta\varepsilon_{mod}$ including this effect shall be calculated as using any one of Eq.(21), Eq.(22), or Eq.(23).

$$\Delta\varepsilon_{mod} = \left(\frac{S^*}{\overline{S}}\right)K^2\,\Delta\varepsilon_{max} \quad (21)$$

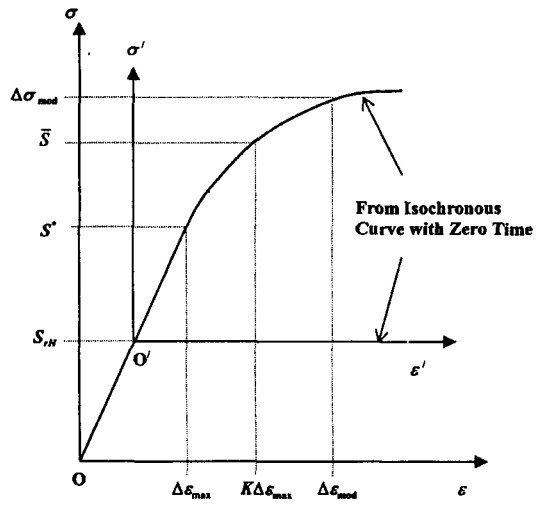

Fig. 15. Composite Stress-Strain Curve for Modified Maximum Strain Range Determination

Table 18. Modified Maximum Equivalent Strain Range (Normal Operation)

Node No	Method-1 $\Delta\varepsilon_{mod} \times 10^{-3}$	Method-3 $\Delta\varepsilon_{mod} \times 10^{-3}$
458	0.558	0.555
976	0.490	0.487
481	0.631	0.620
993	0.362	0.354
797	0.054	0.047
1239	0.042	0.037
1332	0.131	0.127
1344	0.201	0.195
2111	0.021	0.021
2474	0.033	0.033
2502	0.123	0.101
2506	0.428	0.351
2510	0.599	0.593
2748	0.493	0.488
2509	0.031	0.031
2747	0.099	0.097
2729	0.300	0.298
3077	0.272	0.271
3136	0.910	0.904
3086	0.861	0.852

$$\Delta\varepsilon_{mod} = \frac{K^2 S^* \Delta\varepsilon_{max}}{\Delta\sigma_{max}} \quad (22)$$

$$\Delta\varepsilon_{mod} = K_e K \Delta\varepsilon_{max} \quad (23)$$

where S^* and $\bar{S}$ represent the stress indicators and K is the equivalent stress concentration factor as determined by

$$K = \frac{(P+Q+F)_{eff}}{(P+Q)_{eff}} \quad (24)$$

The stress indicators can be determined by using the composite stress-strain curve[12] constructed by adding the elastic stress-strain curve for the stress range, S_{rH} obtained from the relaxation strength analysis, to the appropriate time-independent isochronous stress-strain curve as shown in Fig.15.

Table 17 is the calculated parameters for the modified equivalent strain range. From the table, it is shown that large stress concentrations occur at the junction parts between the support barrel and the baffle plate(nodes 797 and 1239) and between the separation plate and the reactor vessel liner(nodes 2502 and 2506). Table 18 is the modified maximum equivalent strain range obtained using Eq.(21) and Eq.(23).

Finally, the total strain range, ε_t, that is used to enter one of the design fatigue curves of Fig. Y-1420-1 in Ref[3], is calculated as

$$\varepsilon_t = K_v \Delta\varepsilon_{mod} + K \Delta\varepsilon_c \quad (25)$$

In above equation, K_v is the multiaxial plasticity and Poisson ratio adjustment factor, obtained from

$$K_v = 1.0 + f(K_v' - 1.0) \quad (26)$$

where f is the factor determined by using the

Table 19. Calculated Parameters for Total Strain Range (Normal Operation)

Node No.	T.F.	f	$K_e K \Delta_{max} / 3\bar{S}_m$	K_v'	K_v	$\Delta\varepsilon_{mod}$ x 10^{-3}	$\Delta\varepsilon_c$ x 10^{-3}
458	0.54	0.15	0.278	1.0	1.0	0.558	0.000
976	0.48	0.13	0.244	1.0	1.0	0.490	0.000
481	0.20	0.08	0.334	1.0	1.0	0.631	0.400
993	0.40	0.11	0.191	1.0	1.0	0.362	0.400
797	0.59	0.17	0.037	1.0	1.0	0.054	0.003
1239	0.51	0.14	0.029	1.0	1.0	0.042	0.003
1332	0.06	0.01	0.062	1.0	1.0	0.131	0.000
1344	0.70	0.20	0.096	1.0	1.0	0.201	0.000
2111	0.52	0.14	0.018	1.0	1.0	0.021	0.017
2474	0.16	0.07	0.028	1.0	1.0	0.033	0.017
2502	0.39	0.11	0.048	1.0	1.0	0.123	0.000
2506	0.08	0.01	0.174	1.0	1.0	0.428	0.000
2510	0.18	0.08	0.293	1.0	1.0	0.599	0.000
2748	0.58	0.17	0.241	1.0	1.0	0.493	0.000
2509	0.85	0.23	0.017	1.0	1.0	0.031	0.003
2747	0.57	0.16	0.051	1.0	1.0	0.099	0.003
2729	0.62	0.18	0.251	1.0	1.0	0.300	0.010
3077	0.29	0.09	0.228	1.0	1.0	0.272	0.010
3136	0.67	0.19	0.761	1.0	1.0	0.910	0.800
3086	0.14	0.05	0.717	1.0	1.0	0.861	0.800

Triaxiality Factor, T.F., which is defined as

$$\text{T.F.}=\frac{|\sigma_1+\sigma_2+\sigma_3|}{\frac{1}{\sqrt{2}}\left[(\sigma_1-\sigma_2)^2+(\sigma_2-\sigma_3)^2+(\sigma_3-\sigma_1)^2\right]^{1/2}} \quad (27)$$

and K_v' is the plastic Poisson ratio adjustment factor by using the ratio of $K_e K \Delta\varepsilon_{max} E/3\bar{S}_m$.

The creep strain increment $\Delta\varepsilon_c$, corresponding to the stress intensity equal to $1.25\sigma_c$ as defined in Test No. B-1, for the stress cycle due to load-controlled stresses can be determined from the isochronous stress-strain curve. In using the isochronous curve, the stress cycle time, including hold time between transients, shall be used instead of the entire service life. Therefore, the $\Delta\varepsilon_c$ equals the sum of the creep strain increment accumulated in one stress cycle time. Alternatively, the creep strain accumulated during the entire service life divided by the number of stress cycles during the entire service life may be used for the creep strain increment $\Delta\varepsilon_c$.

Table 19 shows the calculated parameters for the total strain range. In this result, the inelastic multiaxial plasticity and Poisson ratio has no effect on the modified maximum equivalent strain because the plastic Poisson ratio factor is 1.0 for all nodal points of interest.

For the fatigue damage evaluation, the number of the cyclic strain history for the thermal load occurring from the hot standby to the steady state operation is assumed as 30 conservatively. Four of the OBEs are assumed to occur during the worst Level A service conditions and one OBE is assumed to occur during the worst Level B service conditions. Each earthquake is assumed to contain 10-peak acceleration cycles.

Table 20. Calculated Fatigue Damages for Service Level A and B

Node No.		Thermal Load (30 Cycles) $K_v \Delta \varepsilon_{mod}$ x 10^{-3}	Thermal Load (30 Cycles) $K \Delta \varepsilon_c$ x 10^{-3}	Thermal Load (30 Cycles) Seismic OBE (50 Cycles) ε_t x10^{-3}	Seismic OBE (50 Cycles) ε_t x10^{-3}	Fatigue Damage $= \sum_{j=1}^{P}\left(\frac{n}{N_d}\right)_j$
Lower SB/SP	458	0.558	0.000	0.556	0.119	0.000
	976	0.490	0.000	0.489	0.120	0.000
Upper SB/SP	481	0.631	0.413	1.030	0.238	0.000
	993	0.362	0.413	0.765	0.233	0.000
SB/BP	797	0.054	0.004	0.051	0.025	0.000
	1239	0.042	0.004	0.041	0.025	0.000
SP/SB	1332	0.131	0.000	0.127	0.169	0.000
	1344	0.201	0.000	0.194	0.161	0.000
BP/SB	2111	0.021	0.017	0.038	0.160	0.000
	2474	0.033	0.017	0.050	0.150	0.000
SP/RVL	2502	0.123	0.000	0.115	0.046	0.000
	2506	0.428	0.000	0.401	0.074	0.000
RVL/SP	2510	0.599	0.000	0.594	0.282	0.000
	2748	0.493	0.000	0.489	0.230	0.000
RVL-Cold Free	2509	0.031	0.003	0.034	0.003	0.000
	2747	0.099	0.003	0.102	0.003	0.000
RVL at BP Elevation	2729	0.300	0.010	0.310	0.002	0.000
	3077	0.272	0.010	0.282	0.002	0.000
RVL- Hot Free	3136	0.910	0.824	1.734	0.000	0.002
	3086	0.861	0.825	1.686	0.000	0.002

Table 21. Calculated Parameters for Creep Damages (Normal Operation)

Node No.		t_H, hrs	t_{HT}, °C	$\bar{t}_j$, hrs	Relaxed stress level at time t S_j	$\bar{S}_r$	G	S_r	S_{LB}
Upper SB/SP	481	262800	430	8760	127.6	125.8	1.00	126.1	160.25
	993	262800	430	8760	123.1	121.6	1.00	121.9	160.25
SB/BP	797	262800	530	8760	9.9	9.8	1.00	9.8	8.88
	1239	262800	530	8760	7.9	7.8	1.00	7.8	8.88
BP/SB	2111	262800	530	8760	7.3	7.2	1.00	7.2	39.13
	2474	262800	530	8760	9.7	9.6	1.00	9.6	39.13
RVL-Cold Free	2509	262800	430	8760	5.5	5.4	0.95	5.4	8.88
	2747	262800	430	8760	16.4	16.0	1.00	16.1	8.88
RVL at BP Elevation	2729	262800	530	8760	59.9	53.5	1.00	54.8	30.25
	3077	262800	530	8760	54.4	49.8	1.00	50.7	30.25
RVL- Hot Free	3136	262800	530	8760	135.8	72.7	1.00	85.3	133.50
	3086	262800	530	8760	134.0	72.0	1.00	84.4	133.50

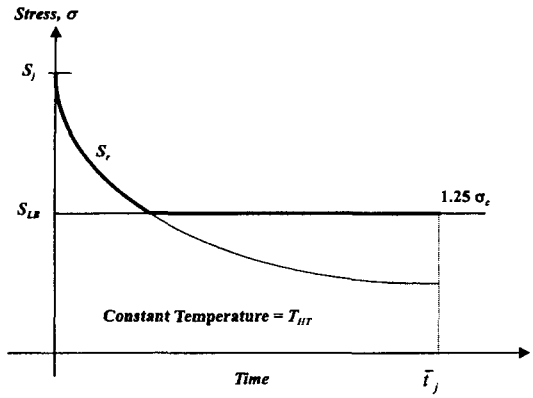

Fig. 16. Concept of Stress Relaxation Limits for Creep Damage Evaluation

Table 20 is the results of the fatigue damage evaluation for the normal operation including the seismic OBE load. The ASME Code fatigue life, i.e. the number of allowable cycles, at the calculated total strains for the thermal load and the seismic OBE is very large (above 10^6) compared to the number of expected Service Level A and B events. Therefore, all points of interest have no fatigue damage for the stress cycles of the normal with the seismic OBE events except small damage for the reactor vessel liner at the hot sodium free surface.

4.3.2. Evaluation of Creep Damage

The creep damage term in Eq.(19) of the creep-fatigue damage equation is to be evaluated using the general procedure provided in ASME Code Case N-201-4.

The total number of hours of the normal operation assumed as Fig.11 is t_H = 262800 hours. Table 21 represents the parameters for the creep damage evaluation. In Table 21, the nodes subjected the elevated temperature for normal operation, which may result in the creep damage, are only selected. The holding temperature of each node, T_{HT}, to be equal to the local metal temperature that occurs during sustained normal operation, is shown in Table 21. With consideration of the total 30-numbers of stress cycle, the average cycle time becomes $\bar{t}_j = t_H / n_j$ = 262800/30 = 8760 hours.

To obtain the stress $(S)_k$ which enters to the minimum stress-to-rupture curve to determine the allowable time duration, the stress level, S_j corresponding to ε_t (Table 20) and T_{HT} from the time-independent isochronous stress-strain curve shall be obtained at first as shown in Table 21. Account for stress relaxation during the average cycle time, the stress relaxation evaluation is to be performed at the constant temperature equal to T_{HT}. This relaxed stress level at time t adjusted for the multiaxial stress state shall be calculated using

$$S_r = S_j - 0.8G(S_j - \bar{S}_r) \tag{28}$$

where S_j is the initial stress level for cycle type j and $\bar{S}_r$ is the relaxed stress level at time t based on a uniaxial relaxation model. G is the multiaxiality factor defined as

$$\frac{[\sigma_1 - 0.5(\sigma_2 + \sigma_2)]}{[\sigma_1 - 0.3(\sigma_2 + \sigma_3)]} \tag{29}$$

where σ_1, σ_2, and σ_3 are principal stresses defined by $|\sigma_1| \geq |\sigma_2| \geq |\sigma_3|$. The values of G greater than 1.0 shall be taken as 1.0.

Table 21 shows the relaxed stress level at time t adjusted for the multiaxial stress state at each node of interest. Fig.16 shows the concept of the stress relaxation limits for creep damage evaluation. As shown in Fig.16, the stress relaxation process shall not be permitted to proceed to a stress level less than S_{LB}. This lower bound stress level, S_{LB}, is defined to be equal to $1.25\sigma_c$ that exits during sustained normal operation. In Table 21, when the lower bound stress level, S_{LB}, exceeds the stress level S_j, it shall be considered that there is no stress relaxation for the creep damage. From the

Table.22 Calculated Creep Damage for Service Level A and B

Node No.		$(T)_k$, ℃	$(S)_k$, MPa	$(\Delta t)_k$ hrs	$(S)_k/K'$, MPa	q	$(T_d)_k$ hrs	Creep Damage $= \sum_{k=1}^{q}\left(\frac{\Delta t}{T_d}\right)_k$
Upper	481	430	127.6	8760	141.8	30	1.0×10^7	0.026
SB/SP	993	430	123.1	8760	136.8	30	1.0×10^7	0.026
SB/BP	797	530	9.9	8760	11.0	30	1.0×10^8	0.003
	1239	530	7.9	8760	8.8	30	1.0×10^8	0.003
BP/SB	2111	530	7.3	8760	8.1	30	1.0×10^8	0.003
	2474	530	9.7	8760	10.8	30	1.0×10^8	0.003
RVL-Cold	2509	430	5.5	8760	6.1	30	Over 10^8	0.000
Free	2747	430	16.4	8760	18.2	30	Over 10^8	0.000
RVL at BP	2729	530	59.9	8760	66.6	30	3.0×10^6	0.088
Elevation	3077	530	54.4	8760	60.4	30	3.0×10^6	0.088
RVL- Hot	3136	530	133.5	8760	148.3	30	3.0×10^5	0.876
Free	3086	530	133.5	8760	148.3	30	3.0×10^5	0.876

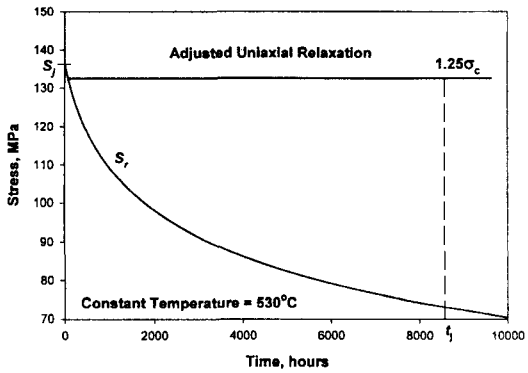

Fig. 17. Stress Relaxation Limits for Creep Damage at Node No.3136

calculated results, the relaxed stress level so small at most node points except at the reactor vessel liner part of the hot pool free surface. However, in these nodes, the stress relaxation severely occurs but S_{LB} value is so high and has almost same stress level of S_j as shown in Table 21. Fig.17 shows the stress-relaxation limits for creep damage at node 3136 for example. From the calculated results of Table 21, it is assumed that the stress $(S)_k$, is same as S_j and the time intervals, $(\Delta t)_k$, is set as 8760 hours conservatively.

For evaluation of the creep damage, the allowable time duration $(T_d)_k$ is obtained from the expected minimum stress-to-rupture curve using the extrapolation. During each of time intervals, $(\Delta t)_k$, the stress, $(S)_k$, is assumed to be constant and is equal to the value at the start of that interval. The allowable time duration $(T_d)_k$, shall be obtained using the $(S)_k$ value divided by the stress factor K' =0.9.

As shown in Table 22, most parts of the reactor internal baffle annulus region have no significant creep damage except of the reactor vessel liner at the hot sodium free surface elevation. The creep damage of reactor vessel liner at the hot sodium free surface is 0.876, which is so large and represents a small design margin for the normal operation. However, this part is not the load

bearing structure but shall be satisfied by the rule of the elevated temperature design for all service loadings.

5. Conclusions

In reactor internal structures, the maximum thermal stresses occur at the junction part of the support barrel and the separation plate due to the large thermal gradients induced by the direct interface between hot pool and cold pool. Even though the wall-averaged temperature in this region is about 430℃ at cycles of normal operation, severe inelastic strains induced by creep and ratcheting phenomena are occurred because of large primary stresses and secondary stresses with the elastic followup and the range of secondary stresses.

At the separation plate, the high bending stresses are occurred due to the thermal gradient through the thickness and also due to the vertical seismic load. Fortunately, the wall-averaged temperature is within the range of ASME Subsection NG.

For the baffle plate, the wall-averaged temperature is so high as 530℃ but the thermal stress is so small. Therefore, it is expected that the creep or ratcheting strain is not severe. However, large bending stresses can be occurred due to the mainly vertical seismic load.

The junction part of the separation plate and reactor vessel liner is also high stress region but the wall-averaged temperature is almost same as that of the cold pool sodium, 386℃. Therefore, it is not necessary to adapt the elevated temperature design rules for this region.

In the reactor vessel liner, the maximum axial thermal gradient is occurred at the elevation of the hot pool free surface. The wall-averaged temperature in this region is about 530℃, therefore the creep and ratcheting strain can be severely accumulated during the total service lifetime. Even the primary stress is not severe in this region as much as to cause the creep and ratcheting strain but the secondary stress with the elastic followup is very large. Therefore, the accumulation of the inelastic strain should be carefully considered in design stage to meet the functional and structural integrity requirements. Severe axial thermal gradient is also occurred at the part of the reactor vessel liner around elevation of the baffle plate, which is the interface region between the hot sodium and the stagnant sodium contained in the baffle annulus structure. The wall-averaged temperature in this region is about 530℃, therefore the creep and ratcheting strain can be accumulated during the total service lifetime. The region of the reactor vessel liner at the elevation of the cold pool free surface, the radial temperature gradient is slightly large compared with other sections but the thermal stress and wall-averaged temperature is not severe.

From the results of the structural integrity using the ASME Code Case N-201-4 for elevated temperature design of the reactor internal structures, high thermal gradient regions of the baffle annulus structure satisfy the code rules of the stress limits with enough margins.

In satisfaction of the deformation and strain limits assuring the structural integrity, the reactor vessel liner part of hot pool free surface region and the junction part between the support barrel and the separation plate do not satisfy the deformation and strain limits with using the elastic analysis method but satisfy the rules with using the simplified inelastic analysis method. However, these parts have so small margins of the inelastic strain accumulated for the total service lifetime of the normal operation. Therefore, more detail analyses and evaluations of the total inelastic strain are needed in next design stage.

From the evaluation of the creep-fatigue damage

for the elevated temperature operation of the Service Level A and B, the fatigue damage is negligible and the creep damage is so small at most regions except of the reactor vessel liner part of hot pool free surface region. However, the reactor internal structures satisfy the creep-fatigue damage with interaction effects of elevated temperature.

The further effort will be concentrated on reducing the thermal stress, the accumulated inelastic strain, and the creep damage for elevated temperature regions in the reactor internal structures either through analyses and tests to better define the thermal environment or through design optimization to relieve the thermal load.

Appendix-A, Determination of Stress Relaxation Strength for 316SS

The two relaxation strengths, S_{rH} and S_{rL}, may be determined by performing a pure uniaxial relaxation analysis starting with an initial stress of $1.5S_m$ and holding the initial strain throughout the time interval equal to the time of service above 427℃. In symbols, the subscripts H and L represent the temperatures at the hot and cold extremes of the stress cycle respectively.

The constitutive equation for the primary creep of 316SS is used as follows:

$$\Delta\varepsilon_{cr} = C_1\left(\frac{\partial\varepsilon_c}{\partial t}\right)\Delta t$$

where

$$\varepsilon_c = \dot{\varepsilon}_m + \frac{C\cdot P\cdot t}{(1+Pt)}$$

$\ln C = -1.35 - 5620/T - 50.6\times10^{-6}\sigma + 1.918\ln(\sigma/1000)$

$\ln P = 31.0 - 67310/T + 330.6\times10^{-6}\sigma - 885.0\times10^{-12}\sigma^2$

$\ln\dot{\varepsilon} = 43.69 - 106400/T + 294.0\times10^{-6}\sigma + 2.596\ln(\sigma/1000)$

The units in above equation should be only absolute temperature, hours, pounds and inches. The valid temperature ranges for above equation are from 800°F to 1300°F and the valid stress range is 0.0 psi $\leq\sigma\leq$ 45 ksi. If the temperature T is less than 800°F, then no creep is expected.

The secondary creep equation of 316SS is given as

$$\Delta\varepsilon_{cr} = C_7\, e^{\sigma/C_8} e^{-C_{10}/T}\Delta t$$

where σ is the equivalent stress.

Acknowledgment

This work has been carried out under the Nuclear R & D Program by MOST.

References

1. ASME Boiler and Pressure Vessel Code Section III, Subsection NG, ASME, (1992).
2. ASME Boiler and Pressure Vessel Code Section III, Subsection NH, ASME, (1995).
3. Cases of ASME Boiler and Pressure Vessel Code, N-201-4, ASME, (1994).
4. Elevated Temperature Structural Design Guide for Class 1 Components of Prototype Fast Breeder Reactor, PNC N241-84-08, PNC, (1984).
5. RCC-MR, Design and Construction Rules for Mechanical Components of FBR Nuclear Islands, AFCEN, (1985).
6. Creep-Fatigue Damage Rules for Advanced Fast Reactor Design, IAEA-TECDOC-933, IAEA, (1996).
7. G.H. Koo, "Design Description of KALIMER Reactor Internal Structures," KALIMER/MS420-DD-01/1998, Rev.A, KAERI, (1999).
8. G.H. Koo, H.Y. Lee, Y.S. Joo, et.al, "Thermal

Stress Analysis and Service Limit Check for KALIMER Reactor Internal Structures," Proceedings of the Korean Nuclear Society Spring Meeting, (1999).
9. G.H. Koo, Y.H. Lee, and B. Yoo, "Seismic Design and Analysis of Seismically Isolated KALIER Reactor Structures," Journal of the Earthquake Engineering Society of Korea, Vol.3. No.1, pp.75-92, (1999).
10. ANSYS User's Manual for Revision 5.5, Volume I and II.
11. G.H. Koo, J.H. Lee, and B. Yoo, "Seismic Buckling Analyses and Service Limit Checks for Cylindrical Shell Structures of KALIMER," Proceedings of the Korean Nuclear Society Autumn Meeting, (1999).
12. L.K. Severud, "Creep-Fatigue Assessment Methods Using Elastic Analysis Results and Adjustments," Transactions of the ASME, Vol.113, pp.34-40, (1991).